Adaptive thresholding of tomograms by projection distance minimization

K. J. Batenburg and J. Sijbers

IBBT Vision Lab
University of Antwerp, Belgium

Abstract

Segmentation is an important step to obtain quantitative information from tomographic data sets. However, it is usually not possible to obtain an accurate segmentation based on a single, global threshold. Instead, local thresholding schemes can be applied that use a varying threshold. Selecting the best local thresholds is not a straightforward task, as local image features often do not provide sufficient information for choosing a proper threshold.

Recently, the concept of *projection distance* was proposed by the authors as a new criterion for evaluating the quality of a tomogram segmentation [1]. In this paper, we describe how Projection Distance Minimization (PDM) can be used to select local thresholds, based on the available projection data from which the tomogram was initially computed.

The results of several experiments are presented in which our local thresholding approach is compared with alternative thresholding methods. These results demonstrate that the local thresholding approach yields segmentations that are significantly more accurate compared to previously published methods, in particular when the initial reconstruction contains artifacts.

Key words: Local thresholding, adaptive thresholding, tomography, projections, PDM, segmentation

1 Introduction

Tomography is a powerful technique for three-dimensional imaging of physical objects, without the need to take the object apart. Projection images of the object are acquired along a range of angles, while rotating around the object. An image of the object (a *tomogram*) is then reconstructed from the series of projection images. Besides its well-known applications in medical imaging, tomography is also an important tool in materials science, microbiology and in industrial applications. In this paper, we focus on tomography of objects that consist of a single material (or tissue, in the medical case). An example of such an object can be seen in Fig. 1, which shows a reconstructed slice of a mouse femur, where the trabecular bone has a rather complex morphology. Such images are commonly used in biomedical bone research [2–5]. Even though the bone density is not perfectly constant, it can still be approximated by a constant density fairly well. An example of an industrial application is the reconstruction of raw diamonds from X-ray projections [6]. If the diamond does not contain any impurities, it consists of a single material of constant density. In materials science, electron tomography is used to study the morphology of homogeneous nanoparticles [7,8].

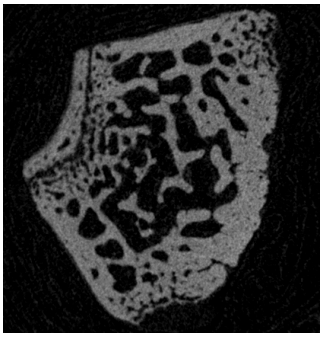

Fig. 1. Reconstructed slice of a mouse femur.

Tomographic reconstructions, which are generally gray-scale images, are often segmented as to extract quantitative information, such as the shape or volume of image objects. Such segmentations are usually performed by global or local thresholding [2–5,7,8]. However, the process of threshold selection is often somewhat arbitrary. A variety of classical algorithms exists for selecting "optimal" thresholds with respect to various optimality measures [9]. Global thresholds are typically selected from the histogram of the image [10–13].

To our knowledge, all previously proposed thresholding methods only use the tomographic reconstruction to select the threshold, while discarding the information contained in the projection data. A reconstructed image, however, generally suffers from various reconstruction artifacts. In materials sciences, for example, where the projection images are acquired using an electron microscope, it is usually not possible to sample the full range of projection angles, which leads to so-called *missing wedge artifacts* in the reconstruction. Also, if the projection of the object falls outside the detector, the reconstruction will suffer from truncation artifacts. To reduce the impact of these artefacts in the selection of the thresholds, Batenburg and Sijbers proposed a new approach for global threshold selection that makes use of the available tomographic pro-

jection data [14,1]. By reprojecting the segmented volume, the norm of the difference between the projections of the current segmentation and the measured projection data, called the *projection distance*, can be computed. This yields a quantitative measure of the quality of the segmentation. By minimizing the difference between the computed and measured projections (*Projection Distance Minimization*, or *PDM*), an optimal threshold can be computed. It was demonstrated in [1], that PDM leads to a significant improvement in segmentation accuracy, compared to histogram-based methods.

However, the capabilities of global threshold selection methods are limited by the maximum accuracy that can be obtained using global thresholding. If the tomogram exhibits variations in the intensity of certain image features, global thresholding can never lead to an accurate segmentation. For example, thick structures typically tend to be brighter than very thin structures in a tomogram, even if both structures consist of the same material in the original object. To account for local image variations, local thresholding methods were proposed. Abutaleb developed a local thresholding method based on the joint (2D) entropy of a pixel neighborhood [15,16]. White and Rohrer developed a nonlinear, local thresholding method in which the gray value of the pixel is compared with the average of the gray values in a small neighborhood [17]. Similarly, the local thresholding method of Niblack adapts the local threshold according to the local mean and standard deviation over a sliding window [18]. Eikvil et al. developed a thresholding method in which a large window, with a small window positioned at its center, is moved across the image, and each pixel inside the small window is labeled on the basis of the clustering of the pixels inside the large window [19]. Blayvas et al. proposed an adaptive binarization method where the threshold is determined by interpolation of the image gray levels at points where the image gradient is high [20].

These adaptive thresholding methods that use a varying threshold for different regions of the image lead to better results than global thresholding in some cases. However, they suffer from the same drawback as global thresholding algorithms in the sense that no objective criterion for the segmentation quality is available if only the information from the reconstructed image is used for segmentation. Moreover, in cases where reconstruction artifacts are not negligible, most adaptive thresholding methods perform even worse than global thresholding methods since adaptive thresholding techniques ar more vulnerable to local variations originating from these artifacts.

In this paper, we propose an extension of the projection-based threshold selection method from [1], that uses a locally varying threshold *field*, instead of a single global threshold. The same optimization criterion, PDM, is now used to find an "optimal" threshold field. The threshold field is represented on a square grid that is coarser than the pixel grid of the tomogram. The thresholds for pixels that do not coincide with grid points in the coarse grid are computed

by bilinear interpolation. Computing the threshold field for which the projection distance is minimal appears to be computationally hard. We describe how a minimum of the projection distance can be computed efficiently for the case that the threshold is only allowed to vary for a single grid point in the coarse grid, while keeping the threshold values fixed for the remaining grid points. By iterating this procedure several times for all coarse grid points, a local minimum of the projection distance is reached. To avoid early convergence to a local minimum that is far away from the global minimum, a stochastic algorithm is proposed which is capable of escaping from local minima before finally converging.

This paper is structured as follows. In Section 2, the local thresholding problem for tomograms is introduced and our local thresholding approach based on PDM is described. Simulation experiments have been performed, comparing the result of local thresholding based on PDM with alternative local thresholding methods and with global thresholding based on PDM [1]. A description of these experiments and their results is given in Section 3. Section 4 concludes the paper.

2 Method

In what follows, we will assume that a reconstruction, containing noise and possible reconstruction artifacts, from an originally binary image is to be segmented. For simplicity reasons, we will restrict ourselves to two-dimensional tomograms. All concepts can be generalized to a 3D setting in a straightforward manner.

2.1 Tomography setting

The grey value image that we want to segment is a tomographic reconstruction of some unknown homogenous object, which can be represented by a function $f : \mathbb{R}^2 \to \{0, 1\}$. We assume that the support of f (i.e., the set $\{(x, y) \in \mathbb{R}^2 : f(x, y) \neq 0\}$) is included in a circle having radius R. Projections are measured along lines $l_{\theta,t} = \{(x, y) \in \mathbb{R}^2 : x \cos\theta + y \sin\theta = t\}$ where θ represents the angle between the line and the y-axis and t represents the coordinate along the projection axis; see Fig. 2.

The *projection function* $P_\theta : \mathbb{R} \to \mathbb{R}$ of f for projection angle θ is defined as

$$P_{\theta,f}(t) = \int_{-\infty}^{\infty}\int_{-\infty}^{\infty} f(x, y)\delta(x \cos\theta + y \sin\theta - t)\,\mathrm{d}x\,\mathrm{d}y. \tag{1}$$

with $\delta(.)$ denoting the Dirac delta function. The function $P_{\theta,f}(t)$ is often called the *Radon transform* of f. Usually, the line projections $P_{\theta,f}(t)$ cannot be measured as continuous functions. Instead, the line projections are measured in a discrete set of t-values as well in a discrete set of projection angles θ.

Suppose now that a tomogram v is reconstructed from the discrete set of projections. Usually, v is represented on a rectangular grid of width w and height h. Put $n = wh$. In what follows, we will assume that v is represented by a vector $\boldsymbol{v} \in \mathbb{R}^n$, where the entries of $\boldsymbol{v}$ correspond to the pixels of the tomogram.

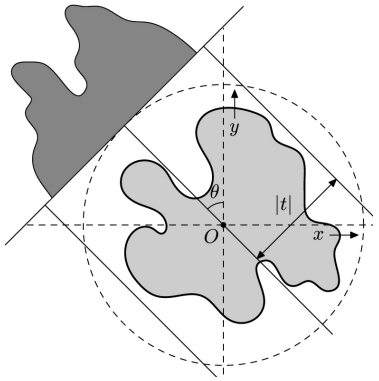

Fig. 2. Basic setting of transmission tomography

2.2 Projection Distance Minimization

As mentioned above, the grey value image $\boldsymbol{v} \in \mathbb{R}^n$ that we want to segment is a tomographic reconstruction of some physical object, of which projections were acquired using a tomographic scanner. Projections are measured as sets of detector values for various angles, rotating around the object. Let m denote the total number of measured detector values (for all angles) and let $\boldsymbol{p} \in \mathbb{R}^m$ denote the measured data. The physical projection process in tomography can be modeled as a linear operator $\boldsymbol{W}$ that maps the image $\boldsymbol{v}$ (representing the object) to the vector $\boldsymbol{p}$ of measured data:

$$\boldsymbol{W}\boldsymbol{v} = \boldsymbol{p}. \tag{2}$$

For parallel projection data, the operator $\boldsymbol{W}$ is a discretized version of the well-known *Radon transform*. We represent $\boldsymbol{W}$ by an $m \times n$ matrix.

For all experiments in Section 3, we used a matrix $\boldsymbol{W}$ for which each row corresponds to a two-dimensional strip through the object, bounded by the left and right side of a detector cell. The entry w_{ij} equals the intersection area between the projected strip i and image pixel j.

From this point on, we assume that an image $\boldsymbol{v}$ has been computed that approximately satisfies Eq. (2). This image now has to be segmented using a locally varying threshold.

In this paper, we focus on the segmentation of objects that consist of a single material, so there are only two segmentation classes, for the object and the background. We assume that the material is homogenous, i.e., a perfect reconstruction of the original object should contain only two grey levels. However, most common tomographic reconstruction algorithms yield an image

that consists of a range of grey levels, instead of a binary image, even if the object in the scanner is perfectly homogeneous. This becomes particularly noticeable if a reconstruction is computed from relatively few projections or if certain parts of the projection data are missing (e.g., truncated projections, where the object is larger than the field of view of the scanner). In such cases, the reconstruction problem is severely underdetermined, and many grey level images can have the same projections. Typically, continuous reconstruction algorithms do not use the prior knowledge about the discrete grey levels, but rather compute an image that contains many grey levels.

Even if prior knowledge about the two grey levels is not used in the reconstruction algorithm, this knowledge can still be exploited by the segmentation algorithm used after reconstruction. Our segmentation approach assigns a single real-valued grey value to both segmentation classes. The projections of the segmented image are then computed and compared to the measured projection data. The difference between the computed and measured projections provides a measure for the quality of the segmentation.

Although we assume that the original object consists of a single material, we do not assume prior knowledge of the actual grey levels of the background and the interior. These grey levels are treated as variables in the segmentation problem. We denote the grey level for the background and the interior of the object by ρ_1 and ρ_2, respectively. Put $\boldsymbol{\rho} = (\rho_1 \ \rho_2)^T$.

We first define a segmentation problem where the local threshold can vary independently for each of the image pixels. The set of local thresholds for all pixels is represented by a vector $\boldsymbol{\tau} \in \mathbb{R}^n$. We will refer to this vector as the *threshold field*.

For any $\boldsymbol{\rho} \in \mathbb{R}^2$, $\tau \in \mathbb{R}$, define the *threshold function* $r_{\boldsymbol{\rho},\tau} : \mathbb{R} \to \{\rho_1, \rho_2\}$ by

$$r_{\boldsymbol{\rho},t}(v) = \begin{cases} \rho_1 & (v \leq \tau) \\ \rho_2 & (v > \tau) \end{cases} . \tag{3}$$

We also define the threshold function $\boldsymbol{r}_{\boldsymbol{\rho},\boldsymbol{\tau}}$ of an entire image $\boldsymbol{v} \in \mathbb{R}^n$, which yields a vector containing the thresholded pixel values:

$$\boldsymbol{r}_{\boldsymbol{\rho},\boldsymbol{\tau}}(\boldsymbol{v}) = (r_{\boldsymbol{\rho},\tau_1}(v_1) \quad \ldots \quad r_{\boldsymbol{\rho},\tau_n}(v_n))^T. \tag{4}$$

For grey levels $\boldsymbol{\rho} \in \mathbb{R}^2$ and a threshold field $\boldsymbol{\tau} \in \mathbb{R}^n$, define the *projection difference* $d(\boldsymbol{\rho}, \boldsymbol{\tau})$ by

$$d(\boldsymbol{\rho}, \boldsymbol{\tau}) = ||\boldsymbol{W}\boldsymbol{r}_{\boldsymbol{\rho},\boldsymbol{\tau}}(\boldsymbol{v}) - \boldsymbol{p}||_2. \tag{5}$$

The projection difference is used as the optimization criterion for finding the optimal threshold parameters. From this point, we will refer to this concept as Projection Distance Minimization (PDM).

Problem 1 *Let $\boldsymbol{W} \in \mathbb{R}^{m \times n}$ be a given projection matrix, let $\boldsymbol{v} \in \mathbb{R}^n$ be a grey level image and let $\boldsymbol{p} \in \mathbb{R}^m$ be a vector of measured projection data. Find $\boldsymbol{\tau} \in \mathbb{R}^n$ and $\boldsymbol{\rho} \in \mathbb{R}^2$, such that $d(\boldsymbol{\rho}, \boldsymbol{\tau})$ is minimal.*

In Problem 1, the threshold for each pixel is allowed to vary independently. This means that the resulting segmentation class for each pixel i (either background or interior) is independent of the grey value v_i, as the threshold τ_i can always be chosen either smaller or larger than v_i. In fact, this threshold selection problem is equivalent to a reconstruction problem from *Discrete Tomography*, where the main objective is to reconstruct a binary image from its projections [21]. Although solving this discrete tomography problem can lead to very accurate segmentation results, even if few projections are used, the problem is computationally very hard (see, e.g., [22]). In cases where it is relatively easy to acquire more projection images, continuous tomography followed by thresholding (either local or global) is often preferable.

At the other end of the granularity spectrum is the case where all entries of $\boldsymbol{\tau}$ must have the same value, i.e., global thresholding. This approach was already proposed in [1]. For binary images, it was demonstrated that only the global threshold τ has to be optimized, as the optimal grey values ρ_1 and ρ_2 can be computed directly once the threshold τ has been set.

2.3 Projection-based local thresholding

In this paper, we focus on a segmentation problem that can be considered as an "intermediate" problem, between discrete tomography and global thresholding based on PDM. Instead of allowing the threshold field $\boldsymbol{\tau}$ to vary independently for each pixel, the value of the threshold is specified on a coarse grid, which is superimposed on the pixel grid of the image $\boldsymbol{v}$. The threshold value for each pixel of v_i is then computed by bilinear interpolation from the set threshold values. In this way, the local thresholds will vary only gradually, while the threshold field can still vary significantly throughout the image. The choice for bilinear interpolation is mainly motivated by computational convenience. More sophisticated interpolation schemes (i.e., bicubic interpolation) may lead to better results. However, such schemes typically yield more variables in the resulting optimization problem.

Fig. 3 illustrates how the coarse grid is superimposed onto the finer pixel grid of the image $\boldsymbol{v}$. Note that only a small portion of the image is depicted. As an example, suppose that the thresholds are given for the four points

indicated in the figure (with corresponding threshold values $\tau_1, \ldots, \tau_4$. Let the (x, y)-coordinates of these four points be given by $(0, 0), (1, 0), (1, 1)$ and $(0, 1)$, respectively. We refer to the four squares between $(0, 0)$ and its surrounding coarse grid points as the *quadrants* surrounding $(0, 0)$. For any pixel p with center (x_p, y_p) in the topright quadrant, the threshold τ_p is defined by bilinear interpolation:

$$\tau_p = (1 - x_p)(1 - y_p)\tau_1 + x_p(1 - y_p)\tau_2 + (1 - x_p)y_p\tau_4 + x_p y_p \tau_3 \quad . \tag{6}$$

Let k be the total number of grid points on the coarse interpolation grid. We refer to the vector of thresholds for these points by $\boldsymbol{\tau'} \in \mathbb{R}^k$. The mapping $I : \mathbb{R}^k \to \mathbb{R}^n$ assigns the corresponding interpolated threshold to each pixel in the fine grid:

$$\boldsymbol{\tau} = I(\boldsymbol{\tau'}) \tag{7}$$

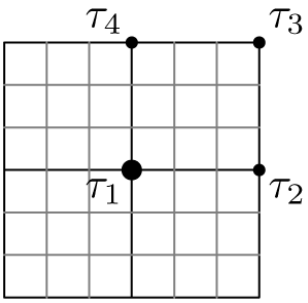

Fig. 3. A coarse grid is superimposed on the finer pixel grid of the reconstructed image.

Using these definitions, we can now formulate the central problem of this paper:

Problem 2 *Let $\boldsymbol{W} \in \mathbb{R}^{m \times n}$ be a given projection matrix, let $\boldsymbol{v} \in \mathbb{R}^n$ be a grey scale image and let $\boldsymbol{p} \in \mathbb{R}^m$ be a vector of measured projection data. Find $\boldsymbol{\tau'} \in \mathbb{R}^k$ and $\boldsymbol{\rho} \in \mathbb{R}^2$, such that $d(\boldsymbol{\rho}, I(\boldsymbol{\tau'}))$ is minimal.*

We will now describe how a constrained version of Problem 2 can be solved efficiently, where only one of the entries of $\boldsymbol{\tau'}$ is allowed to vary, while the remaining entries are kept fixed. Again, consider the example from Fig. 3. Suppose that all thresholds on the coarse grid are kept fixed, except for τ_1. The only pixels for which the thresholds are affected by a change of τ_1 are those in the four quadrants surrounding τ_1, as shown in the figure.

Consider a pixel p with grey level v_p and center (x_p, y_p) in the topright quadrant. Then, taking Eq. (6) into account, the inequality $v_p \geq \tau_p$ is equivalent to

$$g(p) \geq \tau_p \tag{8}$$

with

$$g(p) := \frac{v_p - x_p(1 - y_p)\tau_2 - (1 - x_p)y_p\tau_4 - x_p y_p \tau_3}{(1 - x_p)(1 - y_p)} \tag{9}$$

The $g(p)$ term will be called the *relative grey level of p with respect to τ_1*. This term is different for each of the quadrants surrounding the coarse grid point. Note that $g(p)$ indicates the value of τ_1 at which the segmentation class of p will change, while keeping the other thresholds in the coarse grid

fixed. Therefore, the task of finding a solution of Problem 2 in case only τ_1 is allowed to vary, can be considered as a variant of the global thresholding problem from [1]. In this global thresholding problem, only pixels in the four quadrants surrounding the coarse grid point have to be considered (as the remaining pixels are unaffected by a change of this threshold) and the relative grey level of each surrounding pixel is used instead of the grey levels from $\boldsymbol{v}$.

In [1], an efficient algorithm was presented for finding the optimal global threshold w.r.t. the PDM criterion. The basic idea is as follows. First, the pixels are sorted by their grey level. Starting from the lowest possible threshold, the threshold is gradually increased, while moving pixels from one segmentation class to the other. Each time a pixel is moved, both the optimal grey levels and the corresponding projection distance can be computed efficiently, by performing a small update operation, thereby avoiding a computationally expensive recomputation. For the sake of completeness, we will briefly revisit the approach from [1].

We first describe how the optimal grey levels can be computed for a given segmentation. Let $\boldsymbol{\tau}' \in \mathbb{R}^k$ be the current local threshold field. For $j = 1, \ldots, n$, let $s(j) \in \{1, 2\}$ denote the segmentation class of pixel j. Define $\boldsymbol{A} = (a_{it}) \in \mathbb{R}^{m \times 2}$ by

$$a_{it} = \sum_{j:\ s(j)=t} w_{ij} \quad . \tag{10}$$

Then, the mean squared distance between the projected segmentation $\boldsymbol{A\rho}$ and the measured projection $\boldsymbol{p}$, that is $d(\boldsymbol{\rho}, I(\boldsymbol{\tau}'))^2 = \|\boldsymbol{A\rho} - \boldsymbol{p}\|^2$, is minimized with respect to $\boldsymbol{\rho}$. Classically, the solution of this least squares sense minimization problem is found by solving

$$\bar{\boldsymbol{Q}}\boldsymbol{\rho} = \bar{\boldsymbol{c}} \tag{11}$$

for $\boldsymbol{\rho}$, with $\bar{\boldsymbol{Q}} = \boldsymbol{A^T A}$ and $\bar{\boldsymbol{c}} = \boldsymbol{A^T p}$ (see e.g., Chapter 5 of [23]).

To compute the optimal value of a coarse threshold τ_i', the pixels in the four quadrants surrounding grid point i are first sorted by their relative grey level w.r.t. τ_i'. The threshold τ_i' is then gradually changed, while at each change one or more pixels move from one threshold class to the other class.

Let $\boldsymbol{a_i}$ denote the ith row vector of $\boldsymbol{A}$. Put $\boldsymbol{c_i} = p_i \boldsymbol{a_i}$ and $\boldsymbol{Q_i} = \boldsymbol{a_i a_i^T}$. Suppose that we have computed $\bar{\boldsymbol{c}}$ and $\bar{\boldsymbol{Q}}$ for the current segmentation. We now change the segmentation class $s(j)$ of pixel j. The only rows of $\boldsymbol{A}$ that are affected by this transition are the rows i for which $w_{ij} \neq 0$. This means that the new vector $\bar{\boldsymbol{c}}'$ and matrix $\bar{\boldsymbol{Q}}'$ can be computed by the following updates:

$$\bar{\boldsymbol{c}}' = \bar{\boldsymbol{c}} + \sum_{i:w_{ij}\neq 0} (\boldsymbol{c_i'} - \boldsymbol{c_i}) \tag{12}$$

and

$$\bar{\boldsymbol{Q}}' = \bar{\boldsymbol{Q}} + \sum_{i:w_{ij}\neq 0} (\boldsymbol{Q}'_{\boldsymbol{i}} - \boldsymbol{Q}_{\boldsymbol{i}}) \quad . \tag{13}$$

This update step is independent of the algorithm that is used to compute the segmentation, so it can be used in our new local threshold method without much modification. Fig. 4 shows the basic steps for solving the variant of Problem 2 where only one of the entries of $\boldsymbol{\tau}'$ is allowed to vary. Using the fast update operation, the time complexity of minimizing the projection distance for a single threshold in the coarse grid is reduced to the complexity of computing the forward projection for the four quadrants in all projection directions just once [1].

Computing a global minimum of $d(\boldsymbol{\rho}, I(\boldsymbol{\tau}'))$ as stated in Problem 2 appears to be computationally very hard. In fact, if the coarse grid is taken to have the same resolution as the pixel grid of the reconstructed image, solving Problem 2 is equivalent to solving a variant of the discrete tomography problem. For certain weight matrices $\boldsymbol{W}$, this problem is known to be NP-hard [22].

In [24], the authors proposed a simple iterative algorithm that is guaranteed to converge to a local minimum of the projection distance. In each iteration, a random grid point on the coarse grid is selected. The optimal threshold for this grid point is computed, while keeping the thresholds in all other coarse grid points fixed. The algorithm terminates if no further improvement in the projection distance is obtained after a certain number of iterations. This algorithm was compared to global thresholding based on PDM [1] and the local segmentation algorithm of Niblack [18]. It was shown that the local thresholding based on PDM yields more accurate segmentations than the two alternative methods. A disadvantage of the algorithm proposed in [1], is that the resulting segmentation depends quite heavily on the random order in which the coarse grid points are visited. Without the possibility to continue after reaching a local minimum of the projection distance measure, it may happen that the algorithm gets stuck in a local minimum prematurely, far from the global minimum. To alleviate this problem, we now propose a *stochastic algorithm* which has the ability to leave local minima during the optimization procedure. The algorithm is somewhat similar to simulated annealing: when a threshold in the coarse grid is visited, the optimal value for that threshold is determined. Instead of setting the threshold to that value, a random value sampled uniformly from the interval $[-r, r]$ with $r > 0$ is added to this optimal value. As the iteration counter increases, the parameter r is made progressively smaller, until it finally reaches 0. From that point on, the algorithm behaves exactly the same as the original algorithm from [1]. Fig. 5 shows the algorithmic steps of our stochastic local thresholding method. For all experiments in Section 3, we used $U = 35$ and $C = 768$ as algorithm parameters, which were determined by trial experiments. In experiments we observed that the

Let $\boldsymbol{\tau}' \in \mathbb{R}^k$ be a given vector of thresholds for the coarse grid points and assume that $\bar{\boldsymbol{Q}}$ and $\bar{\boldsymbol{c}}$ have already been computed [1];

Make a list L containing the index j of all pixels in the four quadrants surrounding the coarse grid point i, sorted in ascending order of the relative grey level $g(j)$ w.r.t. i; Denote the size of this list by $|L|$;

Let u be the largest number with $u \leq |L|$ such that $g(L_u) \leq \tau_i'$;

Let $\boldsymbol{\tau}' \in \mathbb{R}^k$ be a given vector of thresholds for the coarse grid points and assume that $\bar{\boldsymbol{Q}}$ and $\bar{\boldsymbol{c}}$ have already been computed [1];

Set $u' := u$; $\bar{\boldsymbol{Q}}' := \bar{\boldsymbol{Q}}$; $\bar{\boldsymbol{c}}' := \bar{\boldsymbol{c}}$;

while $u > 1$ **do**
begin

$u := u - 1$; $\tau_i' := g(L_u)$;
Move pixel L_u from the background class to the foreground class and update $\bar{\boldsymbol{c}}$ and $\bar{\boldsymbol{Q}}$ accordingly;

Compute the minimizer $\boldsymbol{\rho}$ of $d(\boldsymbol{\rho})$ for the current segmentation;

if a new minimum of the projection distance has been found
save the optimal threshold τ_i';

end Set $u := u'$; $\bar{\boldsymbol{Q}} := \bar{\boldsymbol{Q}}'$; $\bar{\boldsymbol{c}} := \bar{\boldsymbol{c}}'$;

while $u < |L|$ **do**
begin

$u := u + 1$; $\tau_i' := g(L_u)$;

Move pixel L_u from the foreground class to the background class and update $\bar{\boldsymbol{c}}$ and $\bar{\boldsymbol{Q}}$ accordingly;

Compute the minimizer $\boldsymbol{\rho}$ of $d(\boldsymbol{\rho})$ for the current segmentation;

if a new minimum of the projection distance has been found
save the optimal threshold τ_i';

end

Fig. 4. Basic steps for finding the optimal threshold in a given coarse grid point i, while keeping the thresholds in all remaining coarse grid points fixed.

stochastic algorithm yields segmentations that are significantly more accurate compared to the non-stochastic version. In addition, the stochastic algorithm appears to be robust with respect to changes in the random seed, as will be demonstrated in the next section.

Compute the optimal global threshold τ, using the algorithm described in [1];

Set $\tau_i' = \tau$ for each point $i = 1, \ldots, k$ on the coarse grid;

for $u := 1$ **to** U **do**
begin
  $r := \lfloor \tau(U-u)/C \rfloor$;
  Generate a random permutation $(\sigma_1, \ldots, \sigma_k)$ of $(1, \ldots, k)$;
  for $j := 1$ **to** k **do**
  begin
    $i := \sigma_j$;
    Compute the value $\tilde{\tau}$ for which the optimal projection difference $d(\boldsymbol{\rho}, I(\boldsymbol{\tau'}))$ is obtained by setting $\tau_i' = \tilde{\tau}$, while keeping the values of the other thresholds fixed;
    Set $\tau_i' := \tilde{\tau} + \text{random}(-r, r)$; (changing the local threshold field);
  end
end

Fig. 5. Basic steps of the threshold selection algorithm. The variables U and C refer to integer constants.

3 Results

Simulation experiments have been performed, starting from four phantom images of size 512×512: a vascular structure (referred to as '*vessel* image'), a *femur* image, a *foam* image, and a *rice* image, which are shown in Fig. 6(a)-(d), respectively. For each experiment, simulated parallel beam projections were computed using equally spaced projection angles. Based on the projection data, three types of reconstructions were computed using the SART algorithm [25]: a *full range* reconstruction with 90 projections, an angle step of 2 degrees, and 512 detector elements; a *missing wedge* reconstruction with 91 projections, an angle step of 1 degree, and 512 detector elements, and a *truncation* reconstruction with 90 projections, an angle step of 2 degrees, and 450 detector elements. The resulting SART reconstructions for the femur and rice phantom image are shown in Fig. 7.

In a first phase, the results of our proposed local PDM thresholding approach were compared with global thresholding. For the global segmentation, we used the PDM algorithm from [1], which computes a global minimum of the projection distance and which was proved to yield significantly better results than conventional global thresholding techniques. The global PDM results are shown in the second column of Fig. 10. Furthermore, the SART reconstructions were segmented using the best possible global threshold that minimizes the number of different pixels between the segmented image and the original

phantom image. This, of course, is only possible with simulation experiments in which the original image is available.

Next, the SART reconstructions were segmented using previously proposed local thresholding methods. A commonly applied adaptive thresholding method was proposed by Niblack [18]; a method that is commonly used as a reference for performance evaluation of local thresholding methods. The Niblack method adapts the local threshold according to the local mean and standard deviation of a sliding window. The method depends on two parameters: the width of the sliding window and the threshold weight of the standard deviation. In practice, these Niblack parameters cannot be optimized because of the lack of "ground truth". In our simulation experiments, in which the "ground truth" was available, we selected the window width and the weight parameter such that the difference between the Niblack segmentation result and the original was minimal. Furthermore, we applied to the SART reconstructions the Minimax local thresholding method, which was recently proposed by Ray and Saha [26]. The method is fully automatic and is based on the minimization of variational energy. Surprisingly, the local thresholding methods performed significantly worse than the global thresholding methods with respect to the pixel error (the number of different pixels between the original image and the segmented result). The reason for this is that local thresholding methods that are solely based on the reconstruction tend to adapt to the reconstruction artefacts in the image, which causes the pixel error to increase. As an example, the Niblack and Minimax thresholding result of the vessel reconstruction are shown in Fig. 8, along with the thresholding result of the global PDM method. It is clear that for this example, the global thresholding outperforms the local thresholding methods. Similar observations were made for all other simulation experiments (visual as well as quantitative evaluation). Hence, global thresholding seems to outperform local thresholding for tomographic reconstructions of binary images. Therefore, in the remainder of this section, we will only show the results of global thresholding and our proposed local PDM method.

Finally, the SART reconstructions shown in the first column of Fig. 10 were segmented using the local PDM thresholding scheme as proposed in this paper. The threshold fields generated by the local PDM method were formed by bilinear interpolation from the threshold values $\boldsymbol{\tau}'$ on the coarse grid.

For all local PDM threshold experiments, a spacing of 16 pixels between consecutive coarse grid points was used to compute the threshold field. The optimal grid spacing can vary depending on image features, number of projections, etc. The spacing of 16 pixels resulted in good reconstruction results over the entire range of experiments. Fig. 9 shows the result of applying our local thresholding approach for the rice phantom (missing wedge case), using a spacing of 4, 16, and 64 pixels, respectively. It can be observed that if the spacing is too small, a form of *overfitting* occurs, while a large spacing does

not allow enough freedom in the threshold field to reduce the missing wedge artifacts.

Table 1 shows the pixel error for the global PDM method, for the method in which the best global threshold was set, and for the local PDM method. The pixel error was computed by comparing the number of different pixels between the thresholded image and the original phantom. On a Pentium IV PC running at 3GHz, the running time of each test was around 30s, consisting of 5s for computing the optimal global threshold and 25s for computing the local threshold field. From Table 1, it is clear that the proposed local PDM thresholding method outperforms the global (and hence also existing local) thresholding methods in terms of the total pixel error.

The thresholding results are also visually shown in Fig. 10. For each phantom image, the SART reconstructions (column 1), the results from the global PDM thresholding method (column 2) and the results from the local PDM thresholding method (column 3) are shown. For the latter method, also the resulting thresholding field is shown (column 4). Note that the deviation from the threshold field mean is a measure for the difference between the global and local PDM thresholding result.

Fig. 11 shows the convergence of our local PDM algorithm for the rice phantom, for the *missing wedge* and *truncated* datasets. In each graph, both the projection distance and the pixel error w.r.t. the phantom are plotted. Note that the iteration count along the horizontal axis refers to the number of local updates performed, for a single threshold in the coarse grid. The graphs show that the projection distance and the phantom error are in fairly good correspondence, which makes the projection distance a suitable criterion for determining the quality of a segmentation.

For practical usefulness of our approach, it is important that the method also works if the scanned object does not correspond perfectly with the binary model. For example, the bone in Fig. 1 is not perfectly homogeneous. We performed simulation experiments for the rice phantom, where i.i.d. additive Gaussian noise was applied to each pixel of the phantom before computing the projection data. The resulting sinogram was then reconstructed using SART and subsequently segmented. Fig. 12 shows the resulting phantoms for three different noise levels, where the noise level (i.e., the standard deviation of the Gaussian distribution) is indicated as a fraction of the maximum grey level in the phantom. Fig. 12 shows the number of misclassified pixels in the segmentation for our local PDM approach and for the best possible global threshold, as a function of the noise level. For noise levels up to 15%, our local threshold algorithm yields more accurate segmentations than global thresholding. For higher noise levels, it appears that some form of *overfitting* occurs in the local threshold approach, so that using a single global threshold becomes preferable.

4 Conclusion

Local grey value thresholding is a common segmentation procedure. However, finding the optimal grey level thresholds is far from trivial. Many procedures have been proposed to select the thresholds based on various image features. Unfortunately, these methods suffer from a clear objective threshold selection criterion.

In our paper, we have presented an innovative approach, called local PDM (Projection Distance Minimization), to find the optimal local threshold grey levels by exploiting the available projection data. Reprojection of the segmented image and subsequent comparison with the measured projection data, yields an objective criterion for the quality of a segmentation. Our approach aims at minimizing the projection distance.

The experimental results show that the proposed local PDM method results in a small difference between the original object and the reconstruction. Simulation experiments were performed for four phantom images, simulating three cases: a full range of projections, a limited range of projections (*missing wedge*) and truncated projection data. In all test cases, PDM clearly leads to significantly better segmentation results than global thresholding based on PDM and much better results than alternative local threshold methods that only make use of information in the reconstructed image itself, while not using the available projection data.

Acknowledgement

This work was financially supported by the F.W.O. (Fund for Scientific Research - Flanders, Belgium)

References

[1] K. J. Batenburg, J. Sijbers, Automatic threshold selection for tomogram segmentation by reprojection of the reconstructed image, in: Computer Analysis of Images and Patterns, Vol. 4673 of Lecture Notes in Computer Science, Springer Berlin / Heidelberg, 2007, pp. 563–570.

[2] M. J. Eichler, C. H. Kim, R. Müller, X. E. Guo, Impact of thresholding techniques on micro-CT image based computational models of trabecular bone, in: ASME Advances in Bioengineering, Vol. 48, 2000, pp. 215–216.

[3] H. R. Buie, G. M. Campbell, R. J. Klinck, J. A. MacNeil, S. K. Boyd, Automatic segmentation of cortical and trabecular compartments based on a dual threshold technique for in vivo micro-CT bone analysis, Bone 41 (2007) 505–515.

[4] A. J. Burghardt, G. J. Kazakia, S. Majumdar, A local adaptive threshold strategy for high resolution peripheral quantitative computed tomography of trabecular bone, Annual Biomedical Engineering 35 (10) (2007) 1678–1686.

[5] K. A. Davis, A. J. Burghardt, T. M. Link, S. Majumdar, The effects of geometric and threshold definitions on cortical bone metrics assessed by in vivo high-resolution peripheral quantitative computed tomography, Calcified tissue international 81 (5) (2007) 364–371.

[6] K. J. Batenburg, A network flow algorithm for reconstructing binary images from continuous X-rays, J. Math. Im. Vision 30 (3) (2008) 231–248.

[7] L. Cervera Gontard, R. E. Dunin-Borkowski, D. Ozkaya, T. Hyde, P. A. Midgley, P. Ash, Crystal size and shape analysis of Pt nanoparticles in two and three dimensions, Journal of Physics Conference Series 26 (2006) 367–370.

[8] D. Ozkaya, A threshold selection method from gray level histograms, Platinum Metals Review 52 (1) (2008) 61–62.

[9] C. A. Glasbey, An analysis of histogram-based thresholding algorithms, Graphical Models and Image Processing 55 (6) (1993) 532 – 537.

[10] T. W. Ridler, S. Calvard, Picture thresholding using an iterative selection method, IEEE Transactions on Systems, Man, and Cybernetics 8 (1978) 630–632.

[11] N. Otsu, A threshold selection method from gray level histograms, IEEE Trans. Syst., Man, Cybern. 9 (1979) 62–66.

[12] A. Rosenfeld, P. Torre, Histogram concavity analysis as an aid in threshold selection, IEEE Trans. Syst., Man, Cybern. 13 (1983) 231–235.

[13] J. Kapur, P. Sahoo, A. Wong, A new method for gray-level picture thresholding using the entropy of the histogram, Comp Vision, Graph, and Image Proc 29 (3) (1985) 273–285.

[14] K. J. Batenburg, J. Sijbers, Automatic multiple threshold scheme for segmentation of tomograms, in: J. M. Pluim, Josien P. W.; Reinhardt (Ed.), Proceedings of SPIE Medical Imaging, Vol. 6512, San Diego, CA, USA, 2007.

[15] A. S. Abutaleb, Automatic thresholding of grey-level pictures using two-dimensional entropies, Pattern Recognition 47 (1989) 22–32.

[16] A. D. Brink, Thresholding of digital images using two-dimensional entropies, Pattern Recognition 25 (1992) 803–808.

[17] J. M. White, G. D. Rohrer, Image thresholding for optical character recognition and other applications requiring character image extraction, IBM Journal of Research and Development 27 (4) (1983) 400–411.

[18] W. Niblack, An introduction to image processing, Englewood Cliffs, New York, 1986.

[19] L. Eikvil, T. Taxt, K. Moen, A fast adaptive method for binarization of document images, in: Proceedings of the International Conference on Document Analysis and Recognition, 1991, pp. 435–443.

[20] I. Blayvas, A. Bruckstein, R. Kimmel, Efficient computation of adaptive threshold surfaces for image binarization, Pattern Recognition 39 (1) (2006) 89–101.

[21] G. T. Herman, A. Kuba (Eds.), Advances in Discrete Tomography and Its Applications, Applied and Numerical Harmonic Analysis, Birkhäuser, Boston, 2007.

[22] R. J. Gardner, P. Gritzmann, D. Prangenberg, On the computational complexity of reconstructing lattice sets from their X-rays, Discrete Math. 202 (1999) 45–71.

[23] G. H. Golub, C. F. Van Loan, Matrix Computations, 3rd Edition, Johns Hopkins University Press, 1996.

[24] K. J. Batenburg, J. Sijbers, Selection of local thresholds for tomogram segmentation by projection, in: Digital Geometry for Computer Imagery, Vol. 4992 of Lecture Notes in Computer Science, Springer Berlin / Heidelberg, 2008, pp. 380–391.

[25] A. C. Kak, M. Slaney, Principles of Computerized Tomographic Imaging, Vol. Algorithms for reconstruction with non-diffracting sources, IEEP Press, New York, NY, 1988, 49-112.

[26] N. Ray, B. Saha, Edge sensitive variational image thresholding, in: IEEE International conference on Image Processing, Vol. 6, 2007, pp. 37–40.

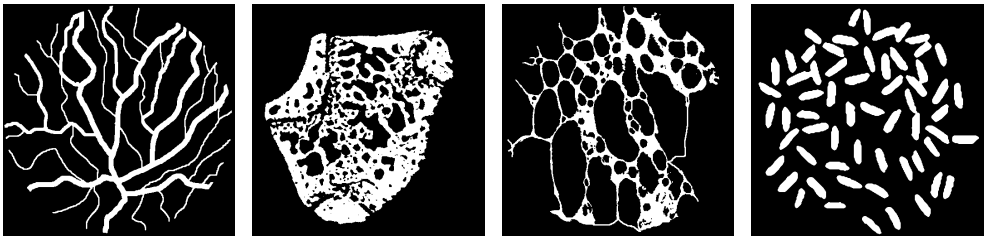

(a) Vessel (b) Femur (c) Foam (d) Rice

Fig. 6. Phantom images used in our simulation experiments: (a) vessel, (b) femur, (c) foam, and (d) rice image.

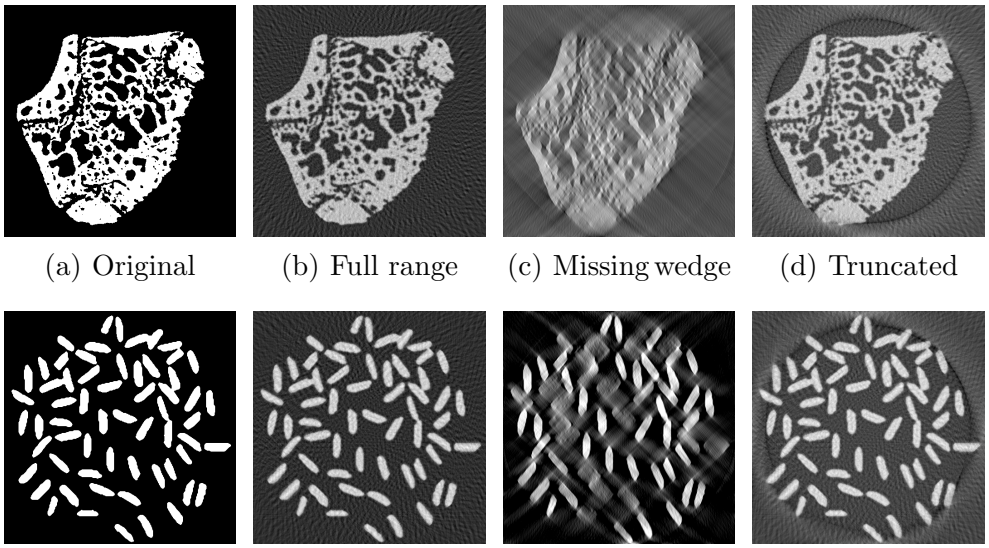

(a) Original (b) Full range (c) Missing wedge (d) Truncated

(e) Original (f) Full range (g) Missing wedge (h) Truncated

Fig. 7. For the femur (row 1) and the rice image (row 2), the original image (column 1), the full projection range reconstruction (column 2), the missing wedge reconstruction (column 3), and the reconstruction from truncated projections (column 4) are shown.

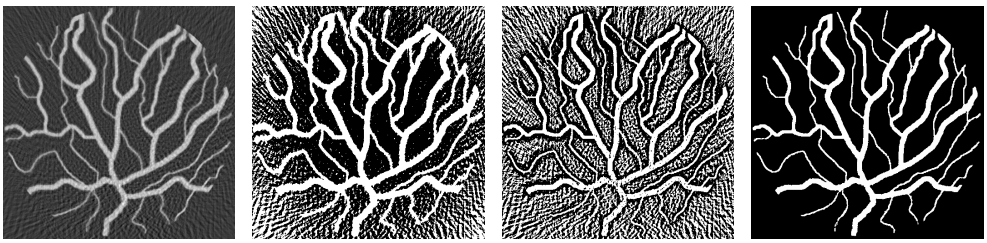

(a) SART (b) Niblack (c) Minimax (d) Global PDM

Fig. 8. Result of local thresholding using the Niblack (b) and Minimax (c) method applied to the SART reconstruction in (a). For comparison, also the result of global PDM thresholding (d) is shown.

(a) 4 pixels spacing (b) 16 pixels spacing (c) 64 pixels spacing

Fig. 9. Results of local PDM for the *rice* phantom (*missing wedge* case) for three different spacings of the coarse grid points.

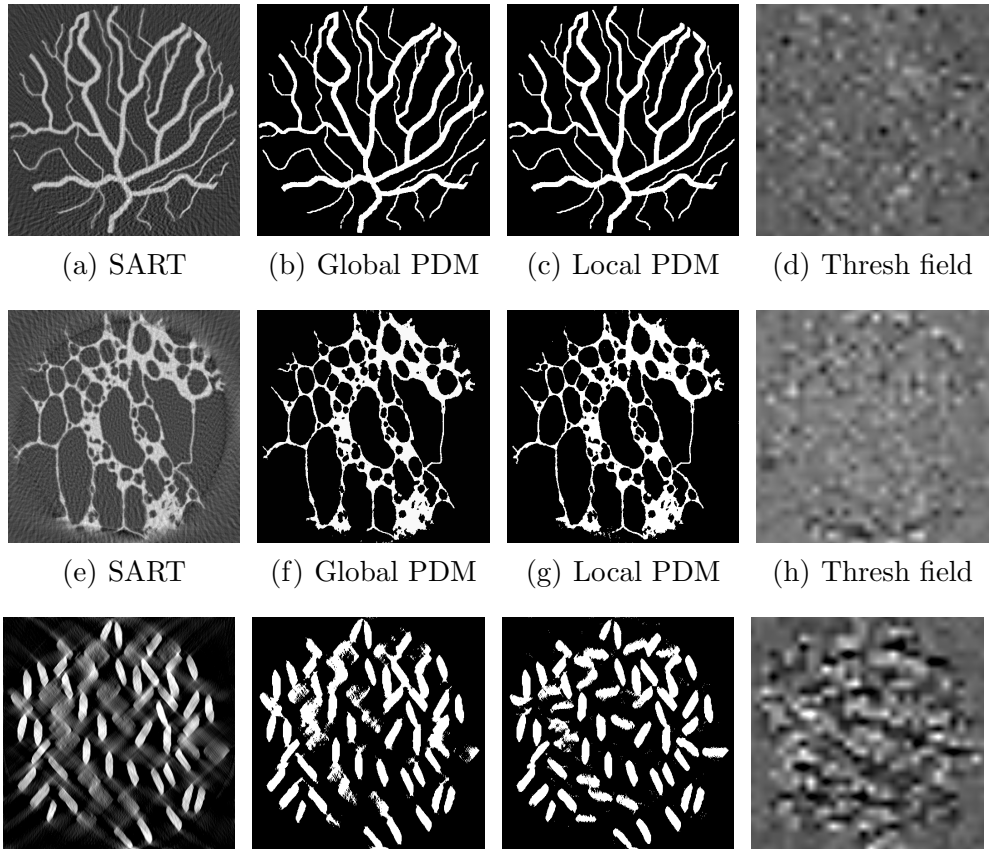

(a) SART (b) Global PDM (c) Local PDM (d) Thresh field

(e) SART (f) Global PDM (g) Local PDM (h) Thresh field

(i) SART (j) Global PDM (k) Local PDM (ℓ) Thresh field

Fig. 10. For the vessel (row 1, all projections), foam (row 2, truncated projections) and rice (row 3, missing wedge) phantom image, the SART reconstruction (column 1), the result of the PDM global thresholding (column 2), the result of the PDM local thresholding (column 3), and the PDM threshold field (column 4) are shown.

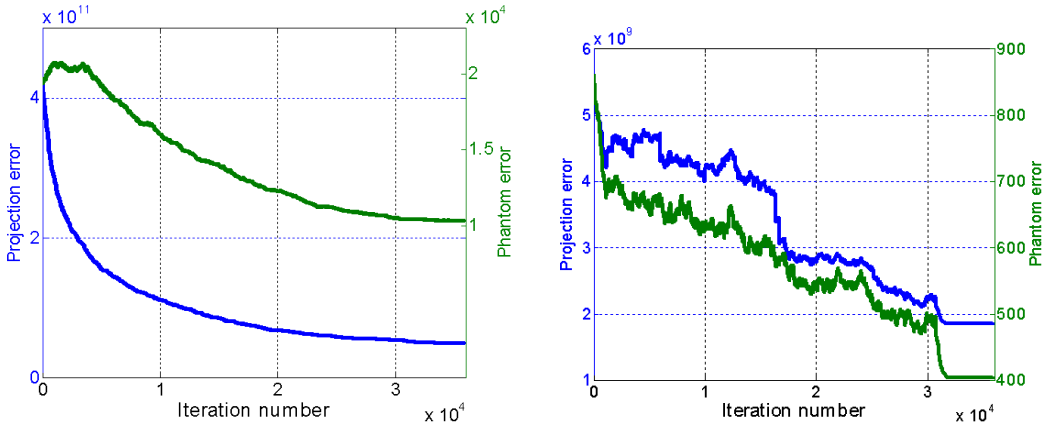

(a) missing wedge (b) truncated

Fig. 11. Convergence graphs for our local thresholding algorithm for the *rice* phantom, for the *missing wedge* and *truncated* datasets. The plots show both the projection distance and the pixel error w.r.t. the original phantom, as a function of the iteration number.

		Global PDM error	**Best global error**	**Local PDM error**
femur	missing wedge	23.666	19.341	18.210 ± 240
	truncated	3.220	3.175	2.212 ± 6
	full range	2.764	2.737	2.039 ± 4
foam	missing wedge	12.113	11.089	9.491 ± 35
	truncated	3.428	3.366	2.284 ± 11
	full range	2.084	2.047	1.407 ± 4
vessel	missing wedge	12.799	12.694	11.950 ± 200
	truncated	2.794	2.652	1.716 ± 5
	full range	1.521	1.502	949 ± 6
rice	missing wedge	19.433	17.736	9.970 ± 220
	truncated	856	854	396 ± 7
	full range	482	476	247 ± 4

Table 1
Comparison of the global PDM method, the best global error and the local PDM method for the femur, foam, vessel, and rice phantom images. For each phantom image, a reconstruction with a missing wedge, with truncation, and with the full angular range was thresholded, after which the number of different pixels with respect to the original image was computed.

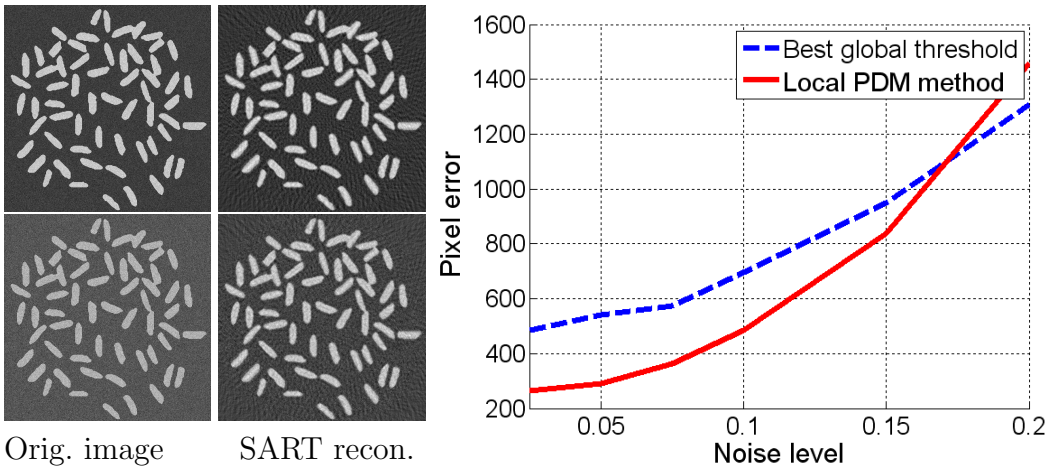

Fig. 12. Left: The rice phantom with noise on the original image (column 1) and the corresponding SART reconstruction (column 2) for a noise level 0.1 (row 1) and 0.2 (row 2). Right: the thresholding error for the best global error and the local PDM method.